Trace Element and Sulfur Isotope Compositions of Gold-bearing Pyrite from the Zhangjiawa Iron Skarn Deposit, Laiwu District: Implications for the Sources of the Early Cretaceous Gold Mineralization in the North China Craton

DUAN Zhuang[1, 2], FU Yangang[1, 2] *, LI Chunjia [3, 4], ZHAO Shaorui [5], GAO Mingbo [3, 4], GAO Jilei [3, 4], JIN Lijie[3,4], LI Siyuan[5] and NGO Dac Xuan[6]

[1.] *Institute of Geophysical and Geochemical Exploration, Chinese Academy of Geological Sciences, Langfang 065000, China*
[2.] *Key Laboratory for Geochemical Exploration Technology, Ministry of Natural Resources, Langfang 065000, China*
[3.] *No.1 Institute of Geology and Mineral Resources of Shandong Province, Jinan 250100, China*
[4.] *Shandong Engineering Laboratory for High-Grade Iron Ore Exploration and Exploitation, Jinan 250100, China*
[5.] *School of Earth Resources, China University of Geosciences, Wuhan 430074, China*
[6.] *Department of Mineral Resource Prospecting and Exploration, Hanoi University of Mining and Geology, Hanoi 100000, Viet Nam*

* Corresponding author. E-mail: fuyg_geology@163.com

Objective

The Zhangjiawa iron deposit is the largest-tonnage and representative iron skarn deposit, with proven reserves of 290 Mt at an average of 46% Fe (up to >65%), in the Laiwu district, eastern North China Craton (NCC) (Fig. 1a,b; Duan et al., 2017). Iron mineralization at Zhangjiawa is mainly hosted along northern contact zone between the Kuangshan dioritic intrusion and Middle Ordovician carbonate rocks that host numerous evaporite intercalations (Fig. 1b,c). The hydrothermal titanite U-Pb dating, showing a weighted mean $^{206}Pb/^{238}U$ age of 131 ± 4 Ma, reveals the Zhangjiawa deposit formed in the early stage of Early Cretaceous (Duan et al., 2017). Magnetite is the major ore mineral, followed by hematite, pyrite and chalcopyrite. Besides high-grade iron ores, copper and cobalt can be of comprehensive utilization, with reserves of 217,256 and 48,548 tons, respectively (Zong et al., 2012).

With further geological exploration, Sanchahe deposit was recently discovered as first medium-sized iron-gold skarn deposit with gold grade of 1.00–24.77 g/t, in the southeastern Laiwu district (Fig. 1b). The Fe-Au orebodies are located near the contact between Tietonggou diorite and Ordovician limestone xenoliths. Native gold mainly occurs in the late sulfide stage, coexisting with pyrite and chalcopyrite at Sanchahe (Ma et al., 2018). The ore-related Tietonggou complex formed during 135–131 Ma (Yang et al., 2006, 2012), which is coeval with the iron skarn mineralization in Laiwu. The new discovery of Sanchahe Fe-Au deposit provides the possibility of reevaluating gold metallogenic potential of the other major iron deposits in Laiwu. In this paper, we report on the newly discovered gold in the Zhangjiawa iron deposit, then carry out in situ composition and sulfur isotope analysis of associated pyrite, which are used to provide insights into the exploration of gold-bearing iron skarn deposits in the western Shandong area, as well as gold sources for the Early Cretaceous gold mineralization in the NCC.

Methods

Sample of sulfide-bearing iron ore (0-22-30) was collected from drill core (ZK0-22) in the Zhangjiawa I mining area. Pyrite grains were handpicked, then mounted in epoxy mounts and polished to expose their interiors. The mount were subsequently examined using optical microscopy, scanning electron microscopy (SEM), and electron probe microanalysis (EPMA), which was conducted using a JXA-8230 Superprobe at the Center for Material Research and Analysis, Wuhan University of Technology.

Trace element concentrations of pyrite were determined using Laser Ablation-Inductively Coupled Plasma-Mass Spectrometry (LA-ICP-MS). The analytical instrumentation employed in this study was a Photon Machines Analyte G2 LA system (193 nm, 4 ns excimer) attached to a PerkinElmer DRC-e ICP-MS, housed at the U.S. Geological Survey (USGS), Denver Federal Center, USA. Spot ablation was carried out using a 30-μm spot size at 5 J/cm^2 and using 7 Hz, with a 35-s baseline and 40 to 50 s of ablation. Ablated materials were transported via an He carrier gas to a modified glass mixing bulb where the He plus the sample aerosol were

This article has been accepted for publication and undergone full peer review but has not been through the copyediting, typesetting, pagination and proofreading process, which may lead to differences between this version and the Version of Record. Please cite this article as doi: 10.1111/1755-6724.14757.

mixed coaxially with Ar prior to the ICP torch. Concentration and detection limit calculations were conducted using the protocol of Longerich et al. (1996). Signals of pyrite were calibrated using USGS MASS-1 sulfide reference material, and iron (^{57}Fe) was used as the internal standard. The reference material (MASS-1) was analyzed five to 10 times at the beginning of the analytical session and monitored throughout the session for drift.

Sulfur isotope analysis were carried out on pyrite using a Nu Plasma II multi-collector inductively coupled plasma mass spectrometer (MC-ICP-MS) system, equipped with a RESOlution S-155 193 nm ArF excimer laser at the GPMR, China University of Geosciences, Wuhan. During the experiment, the diameter of the laser spot was 33 μm with a laser repetition rate of 10 Hz, and the ablation process was set to last for 40 s. The national pyrite standard WS-1 was used in this study. Standard-sample bracketing (SSB) was used to determine the δ^{34}S values of samples throughout the MC-ICP-MS analytical sessions. The true sulfur isotope ratio was calculated by correction for instrumental mass bias by linear interpolation between the biases calculated from two neighboring standard analyses. The analytical precision (2σ) was about ± 0.3 per mil. Detailed analytical conditions and procedures can be seen in Zhu et al. (2016).

Results

Sample 0-22-30 used for this study is an iron ore dominated by magnetite coexisting with phlogopite, which is overprinted with the later pyrite-chlorite-serpentine veins. Calcite in the last stage fills in the fractures and vugs (Fig. 1d). Based on optical characteristics, backscattered electron (BSE) observation and energy dispersive spectrometer (EDS) analysis, native gold and chalcopyrite were recognized, which occur as irregular inclusions about 5 to 50 μm in diameter in pyrite (Fig. 1e–j), implying that minor gold and chalcopyrite are coexisting with pyrite in the sulfide stage at Zhangjiawa.

Major and trace element compositions of gold-bearing pyrite determined by EPMA and LA-ICP-MS from the iron ores are given in Appendix 1. In the 21 trace elements for analysis, only Co, Ni, As and Mn almost can be detected, with the contents of 9316.6–8518.4 ppm, 558.0–1671.8 ppm, 97.3–167.5 ppm and 5.7–8.7 ppm, respectively. High Co and Ni concentrations of pyrite indicate that ore-forming fluids mainly linked to the dioritic or even more mafic deep-seated intrusive rocks. However, the undetectable Au and Cu suggest that these elements are not incorporated into the pyrite crystal lattice, which further supports the fact that the mineral inclusions of chalcopyrite and native gold in pyrite are the main occurring states of Cu and Au at Zhuangjiawa. The similar geological characteristics and occurrences of gold of Zhangjiawa and Sanchahe skarn deposits indicates that Laiwu district should be prospective for the exploration and exploitation of skarn Fe ores with subsidiary gold. Besides, the Fe-Au mineralization-related intrusions at Laiwu were mainly derived from partial melting of the enriched lithospheric mantle and coeval with widespread Early Cretaceous gold deposits (130–120 Ma) in the NCC, which thus provides new evidence that the gold for the craton-scale gold mineralization was sourced from the metasomatized lithosphere mantle of the NCC (Zhu et al., 2015).

Pyrite from the Zhangjiawa iron ore (0-22-30) has δ^{34}S ranging from 17.3 to 18.8‰, which is similar to or even higher than the pyrite δ^{34}S values from the other major iron skarn deposits in Han-Xing and An-Lin districts (Fig. 1k; Appendix 2). Based on the fact of iron orebodies mainly occuring between Mesozoic ore-related intrusions and Ordovician carbonate rocks in North China Craton, these relatively high δ^{34}S values of pyrite suggesting that the sulfur in ore-forming fluids was largely derived from the Ordovician marine sulfates in the wallrocks.

Conclusions

1. Native gold, coexisting with pyrite and chalcopyrite, has been newly discovered in the Zhangjiawa deposit, which is the largest-tonnage iron skarn deposit in the Laiwu district.
2. Gold mainly occurs as mineral inclusions in pyrite instead of incorporation into the pyrite crystal lattice in the Zhangjiawa iron skarn deposit; The high δ^{34}S values of pyrite hosting fine-grained native gold and chalcopyrite, indicate that the sulfur in ore-forimg fluids was largely derived from the Ordovician marine sulfates.
3. The similar geological characteristics and occurrences of gold of the Zhangjiawa and Sanchahe skarn deposits suggests that Laiwu district should be prospective for reevaluating gold metallogenic potential of the other major iron deposits.
4. The occurrences of gold-bearing iron skarn deposits in Laiwu, provide new evidence for the key contribution of gold from the metasomatized lithosphere mantle of the North China Craton.

Acknowledgments

This research was financially supported by the National Natural Science Foundation of China (42002105), Shandong Provincial Bureau of Geology & Mineral Resources (KY201902), China Geological Survey (DD20190571) and Ministry of Science and Technology of China (2012CB416802).

References

Chang, Z.S., Large, R.R., and Maslennikov, V., 2008. Sulfur isotopes in sedimenthosted orogenic gold deposits: evidence for an early timing and a seawater sulfur source. Geology. 36: 971–974.

Duan, Z.,and Li, J.W., 2017. Zircon and titanite U-Pb dating of the Zhangjiawa iron skarn deposit, Luxi district, North China Craton: Implications for a craton-wide iron skarn mineralization. Ore Geology Reviews, 89: 309–323.

Duan, Z., Gleeson, S.A., Gao, W.S., Wang, F.Y., Li, C.J., and Li, J.W. 2020. Garnet U-Pb dating of the Yinan Au-Cu skarn deposit, Luxi District, North China Craton: Implications for district-wide coeval Au-Cu and Fe skarn mineralization. Ore Geology Reviews. 118: 103310.

Li, S.R., Santosh, M., Zhang, H.F., Shen, J.F., Dong, G.C., Wang, J.Z., and Zhang, J.Q., 2013. Inhomogeneous lithospheric thinning in the central North China Craton: zircon U-Pb and S-He-Ar isotopic record from magmatism and metallogeny in the Taihang Mountains. Gondwana Research. 23(1): 141–160.

Longerich, H.P., Jackson, S.E., and Günther, D., 1996. Laser ablation inductively coupled plasma mass spectrometric transient signal data acquisition and analyte concentration calculation: Journal of Analytical Atomic Spectroscopy. 11: 899–904.

Ma, M., and Gao, J.L., 2018. Discovery and Characteristics of Sanchahe Iron Ore Gold Deposit in Laiwu City. Shandong Land And Resources. 34(10): 43–48 (in Chinese with English abstract).

Ouyang, L.M., 2012. Research on geological features, geochemical characteristics and metallogenic prediction for iron deposits in Anyang-Linzhou Area, Henan Province. M.S. Thesis. Central South University, Changsha (in Chinese with English abstract).

Shen, J.F., Santosh, M., Li, S.R., Zhang, H.F., Yin, N., Dong, G.C., and Yu, H.J., 2013. The Beiminghe skarn iron deposit, eastern China: geochronology, isotope geochemistry and implications for the destruction of the North China Craton. Lithos. 156: 218-229.

Wang, Y.J., 2017. The characteristics of Fushan iron deposit, Handan, Hebei province, China, and its implication to the North China Craton evolution. M.S. Thesis. China University of Geosciences, Beijing (in Chinese with English abstract).

Wen, G., Bi, S.J., and Li, J.W., 2017. Role of evaporitic sulfates in iron skarn mineralization: a fluid inclusion and sulfur isotope study from the Xishimen deposit, Handan-Xingtai district, North China Craton. Mineralium Deposita. 52(4): 495–514.

Yang, C.H., Xu, W.L., Yang, D.B., Liu, C.C., Liu, X.M., and Hu, Z.C., 2006. Petrogenesis of the mesozoic high-Mg diorites in west Shandong: evidence from chronology and petro-geochemistry. Earth Science-Journal of China University of Geosciences, 31(1): 81–92 (in Chinese with English abstract).

Yang, Q.L., Zhao, Z.F., and Zheng, Y.F., 2012. Slab–mantle interaction in continental subduction channel: geochemical evidence from Mesozoic gabbroic intrusives in southeastern North China. Lithos, 155: 442–460.

Zhu, Z.Y., Cook, N. J., Yang, T., Ciobanu, C.L., Zhao, K.D.,and Jiang, S.Y. 2016. Mapping of sulfur isotopes and trace elements in sulfides by LA-(MC)-ICP-MS: potential analytical problems, improvements and implications. Minerals. 6(4): 110.

Zong, X.D., Li, W., Wang, J., Qiao, W., Zhang, J.F., and Liu, J.T., 2012. Study on rich iron ore for martin teel and the by-products of Cu and Co in Zhangjiawa iron deposit of Shandong province. Contributions to Geology and Mineral Resources Research. 27(1): 60–65 (in Chinese with English abstract).

Zhu, R.X., Fan, H.R., Li, J.W., Meng, Q.R., Li, S.R., and Zeng, Q.D., 2015. Decratonic gold deposits. Science China Earth Science. 58 (9): 1523–1537.

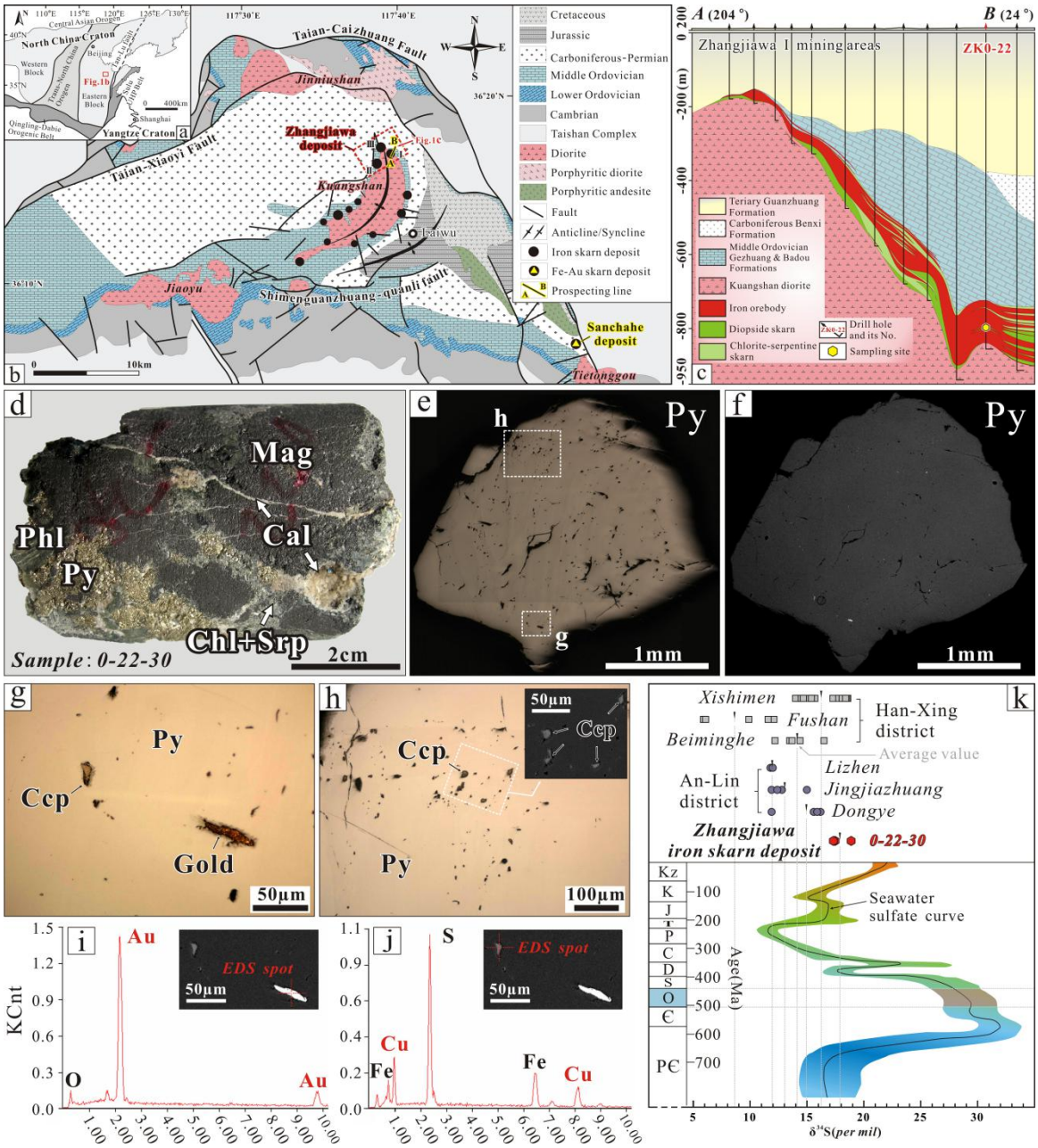

Fig. 1. Geological maps of North China Craton (a) and Laiwu district (b), showing the locations of the Zhangjiawa and Sanchahe deposits (modified from Duan et al., 2017, 2020); A representative cross section in the Zhang I mining area (c); Photograph of hand specimen, reflected-light photomicrographs, BSE images and EDS results of sample 0-22-30 (d-j), showing the occurrences of pyrite, chalcopyrite and native gold; Sulfur isotopic compositions of pyrite from the major iron skarn deposits in North China Craton (k), and the temporal curve for $\delta^{34}S$ values of sulfate seawater are from Chang et al. (2008). Abbreviations: Cal = calcite, Ccp = chalcopyrite, Chl = chlorite, Mag = magnetite, Phl = phlogopite, Py = pyrite, Srp = serpentine.

Appendix 1 Electron probe microanalysis (EPMA) and laser ablation-inductively coupled plasma-mass spectrometry (LA-ICP-MS) analyses of pyrite from the Zhangjiawa iron skarn deposit

EMPA (wt%); Sample: 0-22-30

No.	Fe	Cu	Zn	Au	As	Ni	Co	Cr	S	Total
1	46.02	b.d.l	0.05	b.d.l	0.01	0.04	0.76	b.d.l	53.54	100.43
2	46.65	b.d.l	b.d.l	b.d.l	0.06	0.06	0.16	0.01	53.01	99.96
3	46.76	b.d.l	0.02	b.d.l	b.d.l	0.10	0.14	b.d.l	53.44	100.45
4	45.83	b.d.l	b.d.l	b.d.l	b.d.l	0.04	0.82	b.d.l	53.61	100.31
5	45.99	0.01	b.d.l	b.d.l	0.04	0.08	0.61	b.d.l	53.64	100.38
6	45.18	0.02	0.02	b.d.l	b.d.l	1.00	0.89	b.d.l	53.67	100.78
7	44.64	b.d.l	b.d.l	b.d.l	b.d.l	0.61	1.52	b.d.l	53.47	100.24

LA-ICP-MS (ppm) ; Sample: 0-22-30

No.	V	Cr	Mn	Co	Ni	Cu	Zn	As	Se	Mo	Ag	Cd	Sn	Sb	Te	W	Au	Hg	Tl	Pb	Bi
1	b.d.l	b.d.l	8.3	36438.4	617.5	b.d.l	b.d.l	97.3	b.d.l	b.d.l	b.d.l	b.d.l	b.d.l	b.d.l	b.d.l	b.d.l	b.d.l	b.d.l	b.d.l	b.d.l	0.3
2	b.d.l	b.d.l	b.d.l	85818.4	781.7	b.d.l	b.d.l	121.6	b.d.l	b.d.l	b.d.l	b.d.l	b.d.l	b.d.l	b.d.l	b.d.l	b.d.l	b.d.l	b.d.l	b.d.l	b.d.l
3	b.d.l	b.d.l	6.2	9316.6	1517.9	b.d.l	b.d.l	134.5	b.d.l	b.d.l	b.d.l	b.d.l	b.d.l	b.d.l	b.d.l	b.d.l	b.d.l	b.d.l	b.d.l	0.2	b.d.l
4	b.d.l	b.d.l	5.7	82478.9	558.0	b.d.l	b.d.l	167.5	b.d.l	b.d.l	0.7	b.d.l	b.d.l	b.d.l	b.d.l	b.d.l	b.d.l	b.d.l	b.d.l	b.d.l	b.d.l
5	b.d.l	b.d.l	8.7	56449.6	1671.8	b.d.l	b.d.l	131.0	b.d.l	b.d.l	b.d.l	b.d.l	b.d.l	b.d.l	b.d.l	b.d.l	b.d.l	b.d.l	b.d.l	b.d.l	b.d.l

b.d.l = below detection limit

Appendix 2 Sulfur isotope data for pyrite from the iron skarn deposits in North China Craton

Deposit	Sample	$\delta^{34}S$ (‰)	Reference	Deposit	Sample	$\delta^{34}S$ (‰)	Reference
Han-Xing district				Beiminghe	B-110-6-3	13.5	
Xishimen	XSM2-09	14.3			B-230-2-5	12.2	
	XSM2-12	14.9			B-230-2-3	13.7	Shen et al., 2012
	XSM2-21	15.4			B-245-3	14.4	
	XSM2-01	14			B-245-5	16.5	
	XSM2-07	17.3		An-Lin district			
	XSM-27	15.5		Lizhen	LZ-5	11.8	
	XSM-36	15.7	Wen et al., 2017		LZ-9	12	
	XSM-38	18.6		Jingjiazhuang	JJZ-1	15	
	XSM-29	17.8			JJZ-8	11.9	
	XSM-42	14.5			JJZ-16	12.8	Ouyang et al., 2012
	XSM-43	15.4			JJZ-17	12.4	
	ZK18-1	18.5		Dongye	DY-31	15.6	
	ZK57-1	18.1			DY-32	11.9	
	M89-1	14.7	Li et al., 2013		DY-33	16.2	
	S55-5-2	18.4			DY-34	15.9	
Fushan	F003-3	12.1	Wang et al., 2012	Laiwu district			
	F004-4	6		Zhangjiawa	0-22-30	17.5	
	F006-1	5.9				18.8	This study
	F008-2	6.1				17.3	
	F024-1	9.9					
	XX-3	11.6	Li et al., 2013				